# Alloxan under pressure – squeezing an extremely dense molecular crystal structure

Nicholas P. Funnell, Craig L. Bull, Christopher J. Ridley, Simon Parsons and James P. Tellam

**Published version information**

**Citation:** NP Funnell et al. "Alloxan under pressure – squeezing an extremely dense molecular crystal structure." Chemical Communications, vol. 56, no. 47 (2020): 6428-6431.

**DOI:** 10.1039/D0CC02418J

Journal Name

ARTICLE TYPE

Cite this: DOI: 00.0000/xxxxxxxxxx

# Alloxan under pressure—squeezing an extremely dense molecular crystal structure†

Nicholas P. Funnell,*[a] Craig L. Bull,[a] Christopher J. Ridley,[a] Simon Parsons[b] and James P. Tellam[a]

Received Date
Accepted Date

DOI: 00.0000/xxxxxxxxxx

**The crystal structure of the small organic molecule, alloxan, has been explored using high-pressure neutron diffraction; its already efficiently-packed structure provides a 'chemical head-start' on the pressure experiment. At the highest pressure measured, alloxan reaches a density of 2.36 gcm$^{-3}$—unprecedented for a C, H(D), N, O-containing organic material of appreciable molecular weight. Its crystal structure is stable until ca. 6.5 GPa above which the sample starts to undergo amorphisation.**

The individual intermolecular forces between molecules in a crystal structure determines their spatial arrangment, and consequently, the volume into which they pack. In the organic solid state, molecule–molecule interactions can be dominated by electrostatic contributions if there are electronegative/positive groups that produce strong bond dipoles, such as those involved in typical hydrogen-bonding groups, or if there are even more highly-charged (zwitter)ionic species present.[1] At the other end of the interaction 'spectrum', numerous, dispersive forces can be influential in defining molecular arrangement.[2] Stable crystal structures contain contributions from both these forces to varying extents, depending on the chemical composition. All stable crystal structures are, generally, efficiently packed, thus packing density is a strong consideration in crystal structure prediction when candidate structures are being selected.[3,4] Obvious exceptions to this are porous materials, such as metal-organic frameworks, but for small-molecule structures, minimising volume is important.[5]

Tuning the influence of these interactions, and changing the available volume for molecules to pack into, is readily achieved by applying pressure. It is an effective crystal engineering tool; there are numerous examples where high pressure increases crystal density sufficiently to drive a phase transition through either interaction- or volume-driven instabilities,[6–8] or to bypass kinetic energy barriers entirely via in-situ crystallisation.[9,10] The uppermost achievable pressures are often defined by the experimental setup—the choice of pressure-transmitting medium will constrain the experiment to the intrinsic hydrostatic limit of the fluid.[11] Our approach here for accessing greater pressure-driven density is to use a well-packed, already-dense, molecular crystal to begin with, providing a 'chemical head-start' (for an organic material, in general) on the pressure experiment. We have identified the alloxan crystal structure as being suitable for this. The alloxan molecule (pyrimidine-2,4,5,6-tetraone, shown in Figure 1) is a heterocyclic organic, consisting only of cyclised carbonyl and amino groups.[12] It appears ideally-suited for significant hydrogen-bonding in its crystal structure, yet does not appear to form any 'conventional' hydrogen bonds,[13] although this is not problematic for understanding its stability.[14] At ambient pressure and temperature its crystal structure is tetragonal $P4_12_12$ (and orthorhombic $P2_12_12_1$ below 35 K)[15] and is notable for its rather large density—1.93 gcm$^{-3}$.[16]

Figure 1 shows the density of alloxan in the context of ca. 280000 organic structures in the Cambridge Structural Database,[17] that are comprised of elements lighter than argon, and are free of crystallographic errors and disorder. While its density can largely be attributed to its relatively low hydrogen content—which constitutes just 1.42% of its molecular weight—when contrasted against similar H-weight% materials (<2%), where oxygen is the heaviest atom, alloxan still tends towards the upper end of the resulting distribution (ca. 1000 structures)—see inset graphic in Figure 1a. An alternative crystal packing metric, the Kitaigorodskii index $C_K = Z(V_{mol}/V_{cell})$—unbiased by molecular weight—shows that alloxan is one of the most efficiently-packed structures, having an above-average packing

[a] *ISIS Neutron and Muon Facility, Rutherford Appleton Laboratory, Chilton, U. K.; Tel: +44(0)1235 445385; E-mail: nick.funnell@stfc.ac.uk*
[b] *EaStCHEM School of Chemistry and Centre for Science at Extreme Conditions, University of Edinburgh, The King's Buildings, West Mains Road, Edinburgh, U.K.*

† Electronic Supplementary Information: CIFs for all refined structures, Rietveld fits for all pressures, sample preparation procedure, refinement details for all structures, high-pressure Raman spectra, details of DFT and intermolecular energy computation, compression video, and packing coefficients for analogous $C_{2v}$ molecular crystal structures. CCDC deposition: 1994628–1994636. Data DOI: 10.5286/ISIS.E.RB1620465

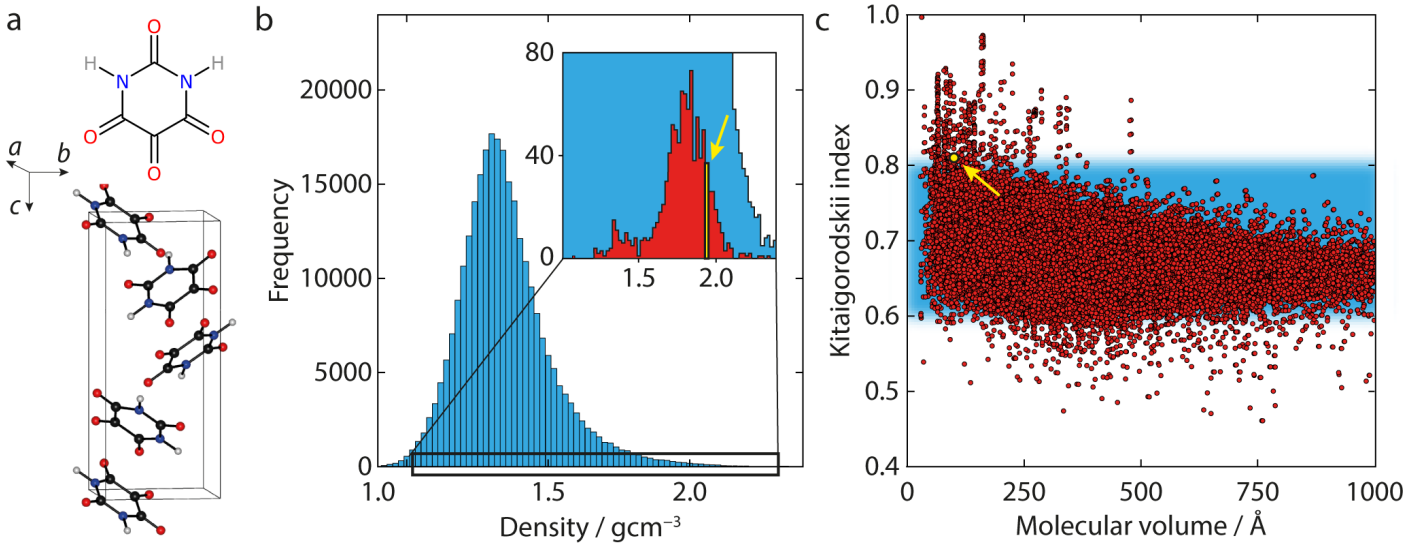


**Fig. 1** (a) Molecular and crystal structures of alloxan (top and bottom); carbon, nitrogen, oxygen and hydrogen (deuterium) atoms are represented by black, blue, red, and white spheres, respectively. Crystal structure CSD Refcode: ALOXAN.[12] (b) CSD-recorded crystal structure densities shown in blue. The inset graphic shows structures with H-weight% $< 2$ in red. The histogram bin in which alloxan is found is shown in yellow, and indicated by the arrow. (c) Kitaigorodskii packing index versus molecular volume—the alloxan datapoint is indicated in yellow.

index of 0.81.[18] Overwhelmingly, organic structures fall in the range 0.6–0.8, indicated by the blue band in Figure 1b.[19] Structures with anomalously low indices may have erroneously calculated molecular volumes or undetermined solvent content, and those with greater indices likely originate from high-pressure structures—vertical arrangements of points are particularly indicative of these. The latter are more prevalent for low molecular volumes, which may reflect the propensity in high-pressure studies for studying relatively simple solids.

Using the already-efficiently-packed alloxan crystal structure as a starting point, we undertook a neutron diffraction experiment to probe its response to application of pressure, at room temperature. Powder diffraction data were collected on the PEARL instrument at ISIS, using argon to compress a deuterated sample (later determined as 25% deuterated) hydrostatically;[20] full details of the sample preparation, high-pressure experimental procedure, and data refinement strategy are given in the S.I. No change in crystal packing was identified up to the highest pressure applied—7.66 GPa—however, sample peaks broadened, as a precursor to eventual amorphisation of the sample. Rietveld refinements were carried out up to 6.49 GPa, owing to a large increase in refined uncertainty on the cell volume at 7.66 GPa. Fits to all powder data, along with refinement statistics are available in the S.I, and crystal structures are provided in CIF format.

The compression behaviour of alloxan is straightforward—the molecules move closer together, predominantly along the tetragonal *c*-axis, and only reorient themselves very subtly, rotating about the crystallographic 2-fold axis running through the molecule, in addition to translation along this axis. A fitted 3rd order Birch-Murnaghan equation of state,[21] using PASCal,[22] gave a bulk modulus ($K_0 = 13.3(14)$ GPa, $K' = 10.8(12)$, and $V_0 = 487.2(19)$ Å$^3$), which is more typical of a hydrogen-bonded organic crystal structure, e.g. L-alanine ($K_0 = 13.1(6)$ GPa and $K' = 7.1(3)$).[23] The large value of $K'$, relative to its usually-assumed value of 4, shows that the crystal structure stiffens rather rapidly with increasing pressure. Plots of cell volume and cell void volume percentage, as a function of pressure, are shown in Figure 2, along with a comparison of the lowest and highest-pressure crystal structures.

The crystal structure is driven towards amorphisation, evidenced by broadening of sample peaks—see Figures in the S.I. The usual explanations for this type of phase transformation can either be the lack of available free volume for molecules to compress into, or the development of destabilising intermolecular contacts. The pressure dependence of the void volume, as a percentage of the unit cell volume (calculated using Mercury CSD 4.0.0) does partially support the former explanation, as the plot trend in Figure 2 appears to be approaching a constant value (ca. 3%) at the highest pressures. The packing efficiency of alloxan improves (necessarily) as cell volume is reduced—$C_K$ increases from 0.81 to 0.92 at 6.49 GPa. This is comparable to benzene where $C_K = 0.92$ at 8.2 GPa, 773 K.[24] However, in materials—like benzene—where relatively deformable H···H dispersion interactions are prevalent, it will be easier for molecules to pack more efficiently. In more electrostatically-dominated materials, e.g. the amino acids, much higher pressures are required to achieve highly-efficient packing; for L-alanine $C_K = 0.93$ at 13.6 GPa,[23] and L-threonine reaches $C_K = 0.98$ at 23.3 GPa.[25] The relative abundance of oxygen, and lack of hydrogen, leads to a large crystal density for alloxan at the uppermost pressures; 2.36 gcm$^{-3}$ by 6.49 GPa, and 2.40 gcm$^{-3}$ by 7.66 GPa. Even compared to other low-H content materials, alloxan is particularly dense; continuously-bonded carbon atoms in graphite produce a density of (2.26 gcm$^{-3}$), and CNO-based energetic materials, noted for their unusually high density, reach 1.94 gcm$^{-3}$.[26,27] In fact, when considering crystal structures in the CSD where oxy-

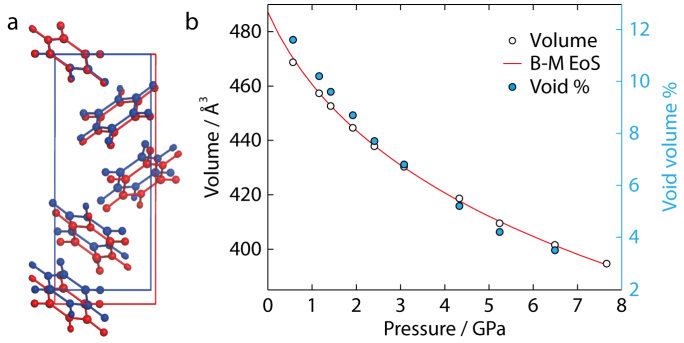


**Fig. 2** (a) View along the *a*-axis showing the spatial arrangement of molecules at ambient pressure (red) and 6.49 GPa (blue). The structures are overlaid exactly at the cell origin. (b) Unit cell volume (open circles) as a function of pressure with the fitted 3rd-order Birch-Murnaghan equation of state (red line). Error bars are within the dimensions of the data markers. The blue markers show the percentage of unit cell volume occupied by empty space.

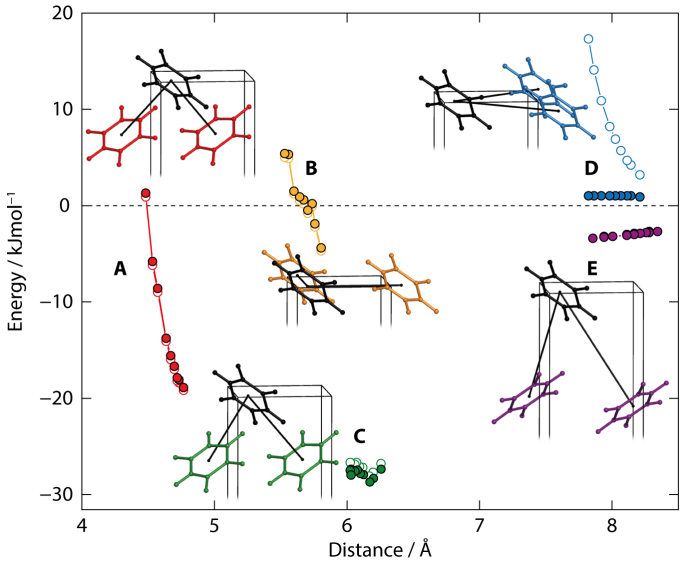


**Fig. 3** Molecule–molecule interaction energies, as a function of centroid distance, are labelled **A**–**E**. Accompanying graphics show the spatial relationship of the relevant molecules (in colour) with the reference molecule (black). As the $C_{2v}$ point symmetry of the molecule is lower than the $P4_12_12_1$ crystal symmetry, there are non-equivalent interaction energies between molecules related by the same space group operation—these are represented by closed and open circles. Most of these are near-degenerate (almost exactly for **E**), except for **D** where the interactions along the [110] and [$\bar{1}$10] directions are very different; the former increases in energy rapidly, as a function of distance. Note that **A** and **C** differ by unit cell translation out of the plane of the page.

gen is the heaviest atom (and filtering out structures with clearly incorrectly-calculated densities), only solid $CO_2$ at 28 GPa is more dense—2.83 gcm$^{-3}$.[28] It appears that among 'moderately-sized' molecules, when under pressure, alloxan becomes the densest C, H, N, O-containing crystal structure recorded to date.

To investigate whether highly-repulsive interactions were occurring, we calculated intermolecular energies using the semi-classical density sums method, implemented in the PIXEL program.[29,30] Details of the PIXEL calculation are available in the S.I. Figure 3 shows the energy of each individual molecule–molecule interaction. Only interactions below ca. 8.5 Å were found to be influential ($>|0.5|$ kJmol$^{-1}$) The PIXEL results show that at the lowest pressure measured (0.57 GPa), all interactions are favourable, except for those aligned along the [110] and [$\bar{1}$10] directions; interaction **D**. The interaction along the [110] direction becomes less stabilising with increased pressure, and eventually, destabilising. This most likely originates from a short O···O contact, decreasing from 2.937 to 2.548 Å; which is difficult for the molecules to avoid as the pertinent carbonyl groups are constrained by symmetry to align with the *ab*-face diagonal. Molecules related by unit cell translation along **a**, and equivalently **b** also become significantly less stabilising at higher pressures. Thus, at the highest pressures measured here, all of the nearest, and next-nearest interactions in the *ab*-plane become destabilising. The greatest change in stability is seen in the shortest interaction **A**, occurring between molecules related by the $4_1$ screw operation, which increases by 20 kJmol$^{-1}$. This interaction is predominantly Coulombic at higher pressure and was previously identified as being influential in cohesiveness of the crystal structure;[14] this is easily understood by mapping its electrostatic potential onto a Hirshfeld surface,[31,32] shown in Figure 4. The favourable alignment between positive (blue) and negative (red) regions of the potential on neighbouring molecules is evident. As a result, the orientation of neighbouring molecules changes very little across the pressures measured here—see S.I. and Supplementary video for further details.

The sharp increase in energy of interaction **A** points toward reduction in stabilising character, which can largely be ascribed to the repulsive component of this interaction, increasing from +28.4 to +86.6 kJmol$^{-1}$. However, as repulsion is the most empirical of the constituent energy components in PIXEL,[5] we performed analogous calculations using CrystalExplorer and Symmetry-Adapted Perturbation Theory (SAPT) approaches to check for consensus (full results in S.I.).[33,34] The CrystalExplorer energies broadly support the PIXEL trends while those from SAPT suggest that the total energy of interaction **A** is relatively unchanged by pressure, originating from large differences in Coulombic and dispersive contributions—ca. 15 and 25 kJmol$^{-1}$, respectively, at high pressure. Although the calculated energy is associated with whole molecule–molecule interactions, and cannot be attributed directly to particular atoms, there is an unusually short C=O···C=O contact formed (the importance of which has been noted in Ref. 16), decreasing from 2.79 Å at ambient pressure (CSD refcode: ALOXAN) to 2.473(5) Å prior to amorphisation, which supports the PIXEL/CrystalExplorer interpretation of the interaction energy. Though this contact is shorter than its more typical distance (ca. 2.7 Å)—ambient pressure alloxan is already close to this—it may be aided by the electrostatic complementarity. This short contact was verified independently using DFT geometry optimisations (in CASTEP—details in S.I.[35]) where it was reproduced in calculations using both fixed, and non-fixed unit cell parameters, resulting in distances of 2.479 and 2.476 Å, respectively. We are not able to detect symmetry-lowering in our diffraction data, which might otherwise provide the molecules

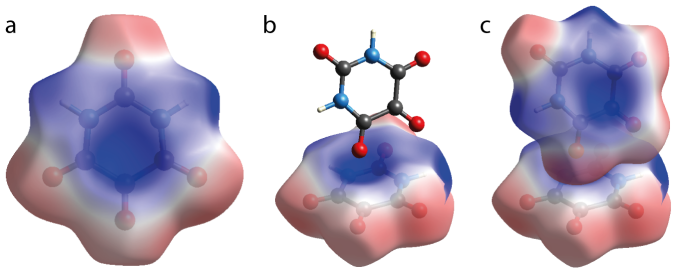


**Fig. 4** Electrostatic potentials mapped on Hirshfeld surfaces. (a) Hirshfeld surface of a single alloxan molecule; positive regions are shown in blue, negative in red. (b) Dimer pair **A**, showing the close C=O···C=O contact. (c) Hirshfeld surfaces of the dimer pair, showing favourable alignment of the molecular electrostatic potentials.

with additional degrees of freedom to avoid the occurrence of this super-short contact. One possibility is that symmetry-lowering distortions could be occurring over a local length scale, and the averaged structure produces the result we measure here, similar to the dynamic collision-avoidance mechanism seen in the plastic phase of cyclohexane,[36] but our data are not sensitive to the subtle background features which would provide this information.

The efficient packing of alloxan could be attributed to its molecular shape as the maximum packing fraction for hard spheroids (0.77) slightly exceeds that of hard spheres (0.74).[37] There is a notable tendency for oblate spheroidal molecules with $C_{2v}$ point symmetry, to crystallise in the $P4_12_12$ or (equivalent) $P4_32_12$ space groups.[14,16,38] Although this packing motif may enable efficient packing of spheroidal objects, all the structures identified in Ref. 14 have quite typical $C_K$ values, falling in the range 0.64–0.74 (see S.I. and Fig. 1b). Visual inspection of the crystal structures using a space-filling representation, in a program such as Mercury CSD, shows that none of the other structures exhibit any significantly-overlapping atomic radii between molecules, but alloxan clearly does, through interaction **A**. It seems alloxan owes its dense packing, under pressure, to a combination of favourable spatial packing and deformable C=O···C=O interactions.

It is clear why the sample amorphises—there is insufficient free volume to support further compression, and intermolecular contacts become repulsive, especially since at least one molecule–molecule contact approaches a distance that is rarely seen. The importance of shape,[23] and electrostatic alignment,[39] on crystal structure compression are already recognised for small molecule systems and, clearly, both of these are factors in the ability of the alloxan crystal structure to support the uppermost density obtained here. Our decision to select alloxan for this study was motivated by its large crystal density, and effective packing at ambient pressure. For further experiments seeking a 'chemical head start' on a pressure experiment, it would be interesting to seek specifically materials that exhibit favourable electrostatic alignment and molecular shapes well-suited to efficient packing, irrespective of their ambient-pressure density and packing coefficient.

## 1 Conflicts of interest

There are no conflicts to declare.

## 2 Acknowledgements

We thank Dr Andrew Maloney for assistance with CSD analysis, and STFC for provision of neutron beamtime.

## Notes and references

1 S. A. Moggach, W. G. Marshall, M. Rogers and S. Parsons, *CrystEngComm*, 2015, **17**, 5315–5328.
2 J. D. Dunitz and A. Gavezzotti, *Chem. Soc. Rev.*, 2009, **38**, 2622–2633.
3 S. L. Price, *Acc. Chem. Res.*, 2009, **42**, 117–126.
4 S. L. Price, D. E. Braun and S. M. Reutzel-Edens, *Chem. Commun.*, 2016, **52**, 7065–7077.
5 A. Gavezzotti, *Molecular Aggregation: Structure Analysis and Molecular Simulation of Crystals and Liquids*, Oxford University Press, Oxford, UK, 2007.
6 S. A. Moggach, W. G. Marshall and S. Parsons, *Acta Crystallogr.*, 2006, **B62**, 815–825.
7 E. Eikeland, M. K. Thomsen, J. Overgaard, M. A. Spackman and B. B. Iversen, *Cryst. Growth. Des.*, 2017, **17**, 3834–3846.
8 P. A. Wood, R. S. Forgan, D. Henderson, S. Parsons, E. Pidcock, P. A. Tasker and J. E. Warren, *Acta Crystallogr.*, 2006, **B62**, 1099–1111.
9 F. P. A. Fabbiani, G. Buth, D. C. Levendis and A. J. Cruz-Cabeza, *Chem. Commun.*, 2014, **50**, 1817–1819.
10 E. L. Smith, J. Ridout, J. D. Sellars and M. R. Probert, *CrystEngComm*, 2019, **21**, 4422–4426.
11 S. Klotz, J.-C. Chervin, P. Munsch and G. L. Marchand, *J. Phys. D: Appl. Phys.*, 2009, **42**, 075413.
12 W. Bolton, *Acta Crystallogr.*, 1964, **17**, 147–152.
13 S. Swaminathan, B. M. Craven and R. K. McMullan, *Acta Crystallogr.*, 1985, **B41**, 113–122.
14 J. D. Dunitz and W. B. Schweizer, *CrystEngComm*, 2007, **9**, 266–269.
15 R. M. Ibberson, W. G. Marshall, L. E. Budd, S. Parsons, C. R. Pulham and C. K. Spanswick, *CrystEngComm*, 2008, **10**, 465–468.
16 T. S. Thakur, M. T. Kirchner, D. Bläser, R. Boese and G. R. Desiraju, *CrystEngComm*, 2010, **12**, 2079–2085.
17 C. R. Groom, I. J. Bruno, M. P. Lightfoot and S. C. Ward, *Acta Crystallogr.*, 2016, **B72**, 171–179.
18 A. I. Kitaigorodskii, *Organic Chemical Crystallography*, Consultants Bureau, New York, 1961.
19 J. D. Dunitz, G. Filippini and A. Gavezzotti, *Helv. Chim. Acta*, 2000, **83**, 2317–2335.
20 C. L. Bull, N. P. Funnell, M. G. Tucker, S. Hull, D. J. Francis and W. G. Marshall, *High Pressure Res.*, 2016, **36**, 493–511.
21 F. Birch, *Phys. Rev.*, 1947, **71**, 809–824.
22 M. J. Cliffe and A. L. Goodwin, *J. Appl. Crystallogr.*, 2012, **45**, 1321–1329.
23 N. P. Funnell, W. G. Marshall and S. Parsons, *CrystEngComm*, 2011, **13**, 5841–5848.
24 A. D. Chanyshev, K. D. Litasov, S. V. Rashchenko, A. Sano-Furukawa, K. Hiroyuki, T. Hattori, A. F. Shatskiy, A. M. Dymshits, I. S. Sharygin and Y. Higo, *Cryst. Growth Des.*, 2018, **18**, 3016–3026.
25 N. Giordano, C. M. Beavers, K. V. Kamenev, W. G. Marshall, S. A. Moggach, S. D. Patterson, S. J. Teat, J. E. Warren, P. A. Wood and S. Parsons, *CrystEngComm*, 2019, **21**, 4444–4456.
26 P. Trucano and R. Chen, *Nature*, 1975, **258**, 136–137.
27 M. A. Kettner and T. M. Klapötke, *Chem. Commun.*, 2014, **50**, 2268–2270.
28 C. S. Yoo, H. Kohlmann, H. Cynn, M. F. Nicol, V. Iota and T. LeBihan, *Phys. Rev. B*, 2002, **65**, 104103.
29 A. Gavezzotti, *J. Phys. Chem.*, 2003, **B107**, 2344–2353.
30 A. Gavezzotti, *Mol. Phys.*, 2008, **106**, 1473–1485.
31 M. A. Spackman, J. J. McKinnon and D. Jayatilaka, *CrystEngComm*, 2008, **10**, 377–388.
32 M. J. Turner, J. J. McKinnon, S. K. Wolff, D. J. Grimwood, P. R. Spackman, D. Jayatilaka and M. A. Spackman, *CrystalExplorer17*, University of Western Australia, 2017.
33 C. F. Mackenzie, P. R. Spackman, D. Jayatilaka and M. A. Spackman, *IUCrJ*, 2017, **4**, 575–587.
34 E. G. Hohenstein and C. D. Sherrill, *J. Chem. Phys.*, 2010, **133**, 104107.
35 S. J. Clark, M. D. Segall, C. J. Pickard, P. J. Hasnip, M. J. Probert, K. Refson and M. C. Payne, *Z. Krist.*, 2005, **220**, 567–570.
36 N. P. Funnell, M. T. Dove, A. L. Goodwin, S. Parsons and M. G. Tucker, *J. Phys.: Condens. Matter*, 2013, **25**, 454204.
37 A. Donev, F. H. Stillinger, P. M. Chaikin and S. Torquato, *Phys. Rev. Lett.*, 2004, **92**, 255506.
38 S. Crawford, M. T. Kirchner, D. Bläser, R. Boese, W. I. F. David, A. Dawson, A. Gehrke, R. M. Ibberson, W. G. Marshall, S. Parsons and O. Yamamuro, *Angew. Chem. Int. Ed.*, 2009, **48**, 755–757.
39 N. Giordano, C. M. Beavers, B. J. Campbell, V. Eigner, E. Gregoryanz, W. G. Marshall, M. Peña-Álvarez, S. J. Teat, C. E. Vennari and S. Parsons, *IUCrJ*, 2020, **7**, 58–70.